



HAL
open science

Endoluminal high-resolution MR imaging protocol for colon walls analysis in mouse model of colitis

Hugo Dorez, Raphaël Sablong, Laurence Canaple, Hervé Saint-Jalmes, Sophie Gaillard, Driffa Moussata, Olivier Beuf

► **To cite this version:**

Hugo Dorez, Raphaël Sablong, Laurence Canaple, Hervé Saint-Jalmes, Sophie Gaillard, et al.. Endoluminal high-resolution MR imaging protocol for colon walls analysis in mouse model of colitis. *Magnetic Resonance Materials in Physics, Biology and Medicine*, 2016, 29 (4), pp.657-669. 10.1007/s10334-016-0539-2 . hal-01296355

HAL Id: hal-01296355

<https://hal.science/hal-01296355>

Submitted on 4 Apr 2016

HAL is a multi-disciplinary open access archive for the deposit and dissemination of scientific research documents, whether they are published or not. The documents may come from teaching and research institutions in France or abroad, or from public or private research centers.

L'archive ouverte pluridisciplinaire **HAL**, est destinée au dépôt et à la diffusion de documents scientifiques de niveau recherche, publiés ou non, émanant des établissements d'enseignement et de recherche français ou étrangers, des laboratoires publics ou privés.

1 **Endoluminal high-resolution MR imaging protocol for colon walls analysis in mouse**
2 **model of colitis**

3
4 Hugo Dorez¹, Raphaël Sablong¹, Laurence Canaple², Hervé Saint-Jalmes^{3,4}, Sophie Gaillard¹,
5 Driffa Moussata^{1,5} and Olivier Beuf¹

6
7 ¹Université de Lyon, CREATIS; CNRS UMR 5220; INSERM U1044; INSA-Lyon,
8 Université Lyon 1, Villeurbanne, France

9 ²Institut de Génomique Fonctionnelle de Lyon, Université de Lyon 1, UMR 5242 CNRS,
10 Ecole Normale Supérieure de Lyon, Lyon, France

11 ³LTSI; INSERM U642; Université Rennes 1, Rennes, France

12 ⁴CRLCC; Centre Eugène Marquis, Rennes, France

13 ⁵Hôpital Régional Universitaire de Tours - Service hépato-gastroentérologie, Tours, France

14
15 SHORT TITLE: Endoluminal MR imaging protocol for mouse colon walls exam

16 Corresponding author:

17 Olivier Beuf, PhD

18 CREATIS, CNRS UMR 5220, Inserm U1044

19 Université Lyon 1, bât. 308 (ESCPE)

20 3 rue Victor Grignard

21 69616 Villeurbanne, FRANCE.

22 Tel: +33 4 72 43 15 97

23 Fax: +33 4 72 44 81 99

26 WORD count of ABSTRACT = 200

27 WORD count of TEXT = 6062

28

29 Number of figures = 7

30 Number of tables = 3

31 Number of references = 53

32

33

34 ACKNOWLEDGMENTS:

35 This work was supported by the LABEX PRIMES (ANR-11-LABX-0063) of “Université de
36 Lyon”, within the program “Investissements d’Avenir” (ANR-11-IDEX-0007) operated by
37 the French National Research Agency (ANR).

38

39

40 ABSTRACT:

41

42 Object: An endoluminal MR imaging protocol including the design of an endoluminal coil
43 (EC) was defined for high spatial resolution MR imaging of mice gastrointestinal walls at
44 4.7T.

45 Materials and Methods: A receive-only radiofrequency single-loop coil was developed for
46 mice colon wall imaging. Combined with a specific protocol, the prototype was first
47 characterized *in vitro* on phantoms and on vegetables. Signal-to-noise ratio (SNR) profiles
48 were compared with a quadrature volume birdcage coil (QVBC). Endoluminal MR imaging
49 protocol combined with the EC was assessed *in vivo* on mice.

50 Results: SNR measured close to the coil is significantly higher (10 times and up to 3 mm of
51 the EC center) than the SNR measured with the QVBC. The gain in SNR can be used to
52 reduce the in-plane pixel size up to $39 \times 39 \mu\text{m}^2$ (234 μm slice thickness) without time penalty.
53 The different colon wall layers can only be distinguished on images acquired with the EC.

54 Conclusion: Dedicated EC provides suitable images for the assessment of mice colon wall
55 layers. This proof of concept provides gain in spatial resolution and leads to adequate
56 protocols, for the assessment of human colorectal cancer that can now be used as a new
57 imaging tool for a better understanding of the pathology.

58

59

60 KEYWORDS: Colorectal Neoplasms, Magnetic Resonance Imaging, Colitis, Instrumentation

61

62 INTRODUCTION:

63

64 Every year, on the overall cases of cancer diagnosed in the world, 13% are colorectal cancer
65 (CRC) [1–3]. It is the second deadliest cancer in Western countries just behind lung cancer.
66 The 5-years survival rate is higher than 80% when the cancer is diagnosed and treated at an
67 early stage [4]. The cancerogenesis of CRC has not been yet precisely established but two
68 major pathways have been identified [5]: the chromosomal instability pathway (adenoma-
69 carcinoma sequence) and the microsatellite instability. Those pathways induce changes in the
70 cellular proliferation with abnormal cells growing and infiltration into the gastrointestinal
71 walls. The different stages of CRC infiltration are well known [6, 7]. It is first characterized by
72 an inflammation stage affecting the superficial layer of the colon wall. Then, the abnormal
73 cells proliferation infiltrates the wall to deeper structures and, eventually, reaches the
74 lymphatic system. Because the survival of patients strongly depends on the diagnosis stage,
75 an early and accurate diagnosis to improve the therapeutic response efficacy is highly beneficial
76 to the patient. Magnetic Resonance Imaging (MRI), computed tomography (CT), positron
77 emission tomography (PET) and some optical modalities provide different kind of information
78 when imaging gastrointestinal walls. However, it is still difficult (using those modalities and
79 associated protocols) to assess fine structures from the abnormal cells proliferation. Today,
80 endoscopic ultrasound (EUS) is widely used in clinical routine for the staging of colorectal
81 cancer lesions [8–10]. It is an available and low cost real-time (motion free) imaging modality.
82 Moreover, the sensitivity of EUS for rectal tumors invasion is approximately 88-95% while
83 specificity is nearly 100% (for stage 2 and more) [11]. However, EUS is especially used on
84 rectal carcinomas and fewer studies have shown the potential of this modality on colon
85 cancer [12–14]. EUS is also strongly dependent on operator and patient and thus require
86 practice to perform an accurate diagnosis. This is especially the case when examination is

87 performed at early stages of CRC. Some studies describe the use of endoscopic MRI
88 compared to EUS [15–19] to assess colorectal region. MRI is well suited to investigate human
89 soft tissues and provides a good spatial resolution for the characterization and staging of
90 gastrointestinal lesions [20]. The modality provides ways of performing high-resolution
91 quantitative maps, various contrast imaging and three-dimensional acquisitions but also
92 performing magnetic resonance spectroscopy. However, colon and rectal walls assessment
93 requires an even higher spatial resolution for visualizing different wall layers in detail [21]. It
94 has been shown that spatial resolution in MRI could be used to depict more precisely, using
95 EC, the gut wall than EUS, for N-staging [17] for example or for the staging of inflammation
96 degrees and cancer lesions. Despite the fact that endoscopic MRI has demonstrated to be
97 superior to MRI using external array coils, by providing exquisite information of wall
98 structures [16, 19, 22, 23], the use of endoscopic coils in human can induce strong local
99 temperature increase at coil tip and along the coaxial cable [24–26]. While heating can be
100 strongly reduced adding for example radiofrequency traps [24, 27], the use of inner coils on
101 humans was currently limited to prostate or rectum and endoscopic MRI of colon based on the
102 use of endoluminal coil is not performed on patient. Especially due to the Human colon
103 anatomy (angle at the rectosigmoid junction) and the invasive procedure (requires anesthesia
104 and insertion of the coil into the patient's rectum).

105 Today, a better understanding of the CRC genesis to adapt therapeutics responses and
106 increase the survival of patients is needed. This goes through the following of the adenoma-
107 carcinoma sequence (inflammation to cancer) on a model of CRC. The follow-up of this
108 sequence on Human longitudinal studies based on endoscopic MRI is not yet possible due to
109 current safety issues. Moreover, the development of CRC on Human is a long process that can
110 last over decades to understand the growth mechanisms (inflammation evolving into cancer).
111 Nevertheless, this can be done on a mouse model of colitis [28], chemically induced by the

112 combination of dextran sulfate sodium (DSS 2% in drinking water) and azoxymethan (AOM,
113 10mg/kg). Trying to understand the growth mechanisms of CRC and to assess the potential of
114 MRI in a mouse model of colitis present several advantages: first, the pathology induced by
115 the method introduced by *Tanaka et al* in 2003 is a reliable model with strong correlations
116 between Human and mice CRC; then, it is possible to follow mice on a much shorter time
117 period (typically six months); and, finally, the examination can be performed for each stages.
118 This paper is describing an endoluminal MRI protocol dedicated to the examination of a
119 mouse cancer model as a preliminary and mandatory step before to move to clinical Human
120 CRC examinations.

121 While MRI is well suited to investigate abdominal-anatomical structures [20], colon and rectal
122 walls assessment requires an even higher spatial resolution for visualizing different wall
123 layers in detail [21], even more on mice (colon wall thickness 0.3-0.7 mm [29]), still within a
124 limited acquisition time suitable for *in vivo* examination.

125 Endoluminal Coil (EC) is drastically increasing the signal-to-noise ratio (SNR) close to the
126 coil compared to external array coil [16, 19, 22, 23]. This kind of elongated loop, based on
127 two coplanar copper traces, was already used for intravascular MRI and MRS in the mid-
128 nineties [30]. The temperature around the EC was measured during *in vitro* acquisition [31].
129 No abnormal and critical temperature increasing was observed. EC can provide a higher
130 spatial and/or temporal resolution and image quality to improve the characterization and
131 staging of colorectal lesions. The aim of this study was to develop, build and characterize an
132 EC for mice rectal wall investigation together with the adapted protocol. The proof of concept
133 of the whole protocol was demonstrated on a limited number of examinations at different
134 stages of a mouse model of CRC.

135

136 MATERIALS AND METHODS:

137

138 **Endoluminal Coil description:**

139 The EC was designed for mice colon investigation on a 4.7 T Bruker Biospec system (Bruker,
140 Ettlingen, Germany). It is a single loop with dimensions sized to the colon mouse
141 anatomy [32] which leads to a 30 mm length and a 1.6 mm outer diameter (heat shrink coating
142 included). The copper tracks are 0.8 mm width and 0.8 mm thick with a copper thickness of
143 35 μm . Following these characteristics, the inductance and resistance of the copper tracks
144 were calculated using the analytical expression of two-distant traces equation. The coil loop
145 and tuning and matching circuit (including a ground plane on the back side of the circuit) were
146 mechanically carved (Circuit Board Plotters S63, LPKF Laser and Electronics®, Germany)
147 on both sides of a FR4 epoxy substrate of 0.8 mm thickness (C.I.F®, Buc,
148 France). Nonmagnetic electronic circuit components were soldered on a single face. The two
149 longest conductors of the loop have been placed on each side of the substrate. A copper tape
150 was used at the distal end of the coil to close the loop between the two faces (Fig 1). One for
151 connecting the loop to the upper face (straight arrows) and, the second one, to connect the
152 direct current (DC) ground and radiofrequency (RF) signal ground together (dashed arrows) to
153 the ground plane. This is done to avoid current loops between two different grounds. The RF
154 signal was carried out by a coaxial cable (RG-58, Radiall®, France) and the DC current
155 travels through a 8-wires cable (Alpha Wire®, New Jersey, USA) connected on a non-
156 magnetic Fisher connector (Plugs 4032, Fisher Connectors®, Suisse) to the coil. This latter
157 decoupling cable is connected to the 14 pins connector of the Bruker decoupling box cable
158 through a homemade Fisher-Bruker conversion cable. A heat shrink coating (PF3-135) houses
159 the loop coil to isolate the tracks from colon and rectum tissues. The end of the coil was sealed
160 with glue (Araldite PRECISION, Araldite®, Bâle, Switzerland). When the EC is used, the

161 electrical circuit is isolated with polytetrafluoroethylene (PTFE or Teflon, DuPont®,
162 Wilmington, USA) to avoid contacts with tissues or liquids.

163

164 **Endoluminal Coil characterization:**

165 The resonant circuit is based on a RLC resonator circuit made of fixed nonmagnetic
166 components (ATC, Huntington Station, New York, USA) and trimmer components
167 (AT 57290, Temex Ceramics®, Bordeaux, France) – Fig 1. Considering only the intrinsic
168 parameters of the coil, which are the coil geometry, the materials used and the coupling
169 effects (mutual inductance for example); the loop inductance and resistance were estimated to
170 33.2 nH and 0.1 Ohm respectively. The values were calculated and corrected using
171 measurements on a Vector Network Analyzer (E5070B – ENA Series, Agilent
172 Technologies®, California, USA) - VNA. Intrinsic characteristics of electronic components
173 (series resistances, self-inductances, parallel capacitances, self-frequency resonance) were
174 modeled to simulate the precise electronic behavior of the coil. Modeling was done using a
175 Simulation Program with Integrated Circuit Emphasis (LTspiceIV, Linear Technology®,
176 Milpitas, USA) feed with electronic components characteristics based on their individual
177 datasheets. The value and manufacturers of the electronic components are summarized in
178 table 1.

179 In the coil design, there are basically four functions to achieve. Briefly, the capacitor C_t insures
180 the tuning function, changing this value adjust the resonance frequency of the coil (on the S11
181 magnitude chart). Capacitors $C_{m,1}$ and $C_{m,2}$ are used for matching the coil to the 50 Ohms
182 impedance of receiver circuit in order to maximize the signal power transmission. The $C_{B,1}$
183 and $C_{B,2}$ capacitors are used for blocking the DC current into the loop coil to improve the
184 decoupling efficiency. It could also create a local static magnetic field interfering with the
185 static magnetic field B_0 . This ensures the correct decoupling of the loop coil. Mounted in

186 series with C_t , capacitors can also contribute marginally for tuning the coil. Trimmer
187 capacitors can be tuned mechanically with a nonmagnetic screwdriver to adjust the coil to
188 match to 50 Ohms at the working frequency of 200 MHz (proton resonance frequency at
189 4.7 T). Finally, the decoupling circuit is represented by two Choke inductors and one PIN
190 diode. The Choke inductors $L_{B,1}$ and $L_{B,2}$ protect the receiver amplifier from the induced RF
191 current during the RF transmit pulses.

192 The PIN diode was mounted in parallel to the loop coil to minimize the series resistance and
193 so maximizes the Quality factor (Q-factor) and thus the SNR [33, 34]. The quality factor of the
194 coil was measured using a Vector Network Analyzer (VNA). The loaded Q-factor Q_L was
195 measured with the EC inserted into a phantom containing a solution of saline solution and the
196 unloaded Q-factor Q_0 was measured without the phantom.

197

198 **SNR assessment:**

199 All the experiments were performed on a 4.7 T Bruker Biospec System (Bruker, Ettlingen,
200 Germany). In order to characterize the EC, each acquisition done with the EC was also
201 compared to a ^1H 32 mm inner diameter quadrature volume birdcage coil (Rapid
202 Biomedical®, Rimpar, Germany) – QVBC dedicated to mouse body. However, the QVBC
203 used does not include any decoupling circuit. As a consequence, the EC should not be inserted
204 within the sample during QVBC operation. That is the reason why, when using the QVBC, an
205 optical fiber (HCG 600, OFS®, Atlanta, USA) surrounded by a heat shrink coating was
206 inserted into the mouse rectum instead of the EC. The outer diameter of the optical fiber and
207 the heat shrink coating is 1.6 mm. Then, when using the EC, the QVBC was replaced by a ^1H
208 72 mm inner diameter transmit linear volume coil (Rapid Biomedical®, Rimpar, Germany) –
209 VC including an active decoupling circuit. A protocol was developed and optimized for the
210 purpose of EC assessment on phantom and small animals. Three axial 3D fast low-angle-shot

211 (FLASH) sequences were used for anatomical and structure imaging but also for computing
212 parametric T1 maps [37]. Then, one coronal FLASH 3D Slab sequence is performed to assess
213 the colon along the EC. Finally, for computing parametric T2 maps, a 2D multiple spin-echo
214 sequence was carried out. Table 2 summarizes the sequences parameters used in the
215 *in vivo* protocol.

216 For SNR gain assessment, the coil was inserted into a 12 mm outer diameter tube filled with a
217 solution of 1.25 g/L of $NiSO_4$ and 5 g/L of $NaCl$ to mimic approximately the loading
218 conditions found in living tissues and have convenient relaxation times (T1-value of 218 ms
219 and T2-value of 140 ms). First, the receiver EC was placed at the center of the VC used in
220 transmit mode. The EC was driven by the active decoupling circuit during transmission. For
221 SNR comparisons, axial images were acquired using FLASH 3D Slab sequences (table 3).
222 Then, VC and EC were replaced by the QVBC and the optical fiber, respectively. With the
223 same protocol, MR images were acquired using the QVBC (emission/reception mode). Slab
224 was positioned manually to scan the same region in order to allow co-localization. The SNR
225 were compared after correcting for difference in voxel size including the antialiasing steps,
226 receive bandwidth and number of excitations between the EC and VCs [38]. SNR profiles were
227 normalized using this method and plotted in the same graph.

228

229 **Spatial resolution and contrast enhancement using an EC:**

230 The improvement of SNR provided by the EC can be used to decrease the voxel size without
231 acquisition time penalties. To assess the spatial resolution achievable in the region of interest
232 (ROI) with the EC within a reasonable acquisition time, a phantom containing the same
233 $NiSO_4$ solution was filled with optical fibers of standard diameters (ranging from 150 μm to
234 1000 μm). Using the transmit VC and the EC in reception mode, two sequences were
235 acquired. First, an axial FLASH 3D Slab with a pixel size of $83 \times 83 \mu m^2$ (slice of 234 μm

236 thick) was carried out(sequence 1 in table 3). Then, the sequence was adjusted to reduce the
237 voxel size up to $39 \times 39 \mu\text{m}^2$ keeping a slice thickness of $234 \mu\text{m}$ (sequence 2 in table 3). The
238 structures observed were measured using the software ImageJ [39]and compared to the optical
239 fiber diameters measured with a digital caliper.

240 After having characterized the ECs on inorganic phantoms, experiments were carried out on
241 organic phantoms such as onions in order to evaluate the sensitivity of such coils.Onions offer
242 fine lamellar structures divided in several bulbs inside. The thickness of the different layers is,
243 in average, the same as the one expected in mouse colon wall. Images performed on
244 vegetables provide good markers to evaluate the sensitivity of the coil by analyzing the finest
245 structure observable (for a given SNR).Experiments were performed using 3D Slab FLASH
246 sequences (20 mm FOV, 25 mm slab thickness, TR/TE = 25/4.31 ms with 25° flip angle,
247 $256 \times 192 \times 96$ matrix, 36 764 Hz bandwidth and 11'31'' acquisition time). The VC was turned
248 in emission mode and the EC switched on reception mode.Finally, the spatial resolution was
249 increased by reducing the pixel size down to $39 \times 39 \mu\text{m}^2$ (10 mm FOV, 15 mm slab thickness,
250 TR/TE = 20/6.1 ms with 20° flip angle, $256 \times 256 \times 64$ matrix, 25 kHz bandwidth and
251 10'55'' acquisition time) with a slice thickness equals to $234 \mu\text{m}$.

252

253 ***In vivomouse colon examination:***

254 *In vivo* experiments wereperformed to evaluate the feasibility and interest of using an EC in a
255 mouse model of colitis.The study was carried out on mice chemically treated during two
256 months to induce colitis using a combination of azoxymethan (AOM, intraperitoneal
257 injection, 10 mg/kg body weight) and dextran sulfate sodium (DSS, in drinking water,
258 concentration of 2%) and four mice without treatment used as control.The experiments were
259 in accordance with the rules and regulations of the UCBL Ethics Committee on animal
260 experimentation. Prior to the examination, mice were kept on a 12 hours day/night rhythm in

261 a 300 cm² plastic cages with straw bedding, pellet food and tap water. Mice were anesthetized
262 using an isoflurane tabletop station (TEM Sega®, Lormont, France). Animals respiratory
263 index was monitored during the experimentation by using a pressure sensor placed on the
264 mouse chest. During the induction phase, mice were anesthetized with 3% of isoflurane and
265 aspiration flow set up on 0.4 L/min. During imaging, the anesthesia was maintained with
266 1.4 to 1.7% isoflurane vaporization and aspiration flow set up on 0.4 L/min. Images of colon
267 wall were first acquired by using the transmit/receive QVBC. In that case, to mimic the
268 presence of the EC, an optical fiber was carefully introduced into the mouse rectum using
269 sterilized lubricant KY gel (K-Y®, Johnson & Johnson, USA) and held in position with
270 adhesive tape (strap on the MRI bed). Then, to assess colon wall layers with the EC, the
271 QVBC was replaced by the linear VC. MR images were acquired to assess colon wall layers
272 using described protocol in table 2.

273 For each animals, T1- and T2-maps were computed using a linear fit from sequences acquired
274 at different flip angle (15°, 20°, 25°) [37] and an exponential fit [40] at six different echo
275 times (12.8 ms, 25.21 ms, 37.81 ms, 50.42 ms, 63.03 ms and 75.63 ms), respectively. Before the
276 computation, images were threshold with an automatic method. The threshold level was set to
277 three times the standard deviation measured in a ROI with no signal (located in the top left
278 corner of the image far from the EC). Two additional maps, representing the T1 linear fit
279 quality and the T2 exponential fit quality, were also computed. To ensure reliable values of
280 T1 and T2 relaxation times, fits having a coefficient of determination (R^2) inferior to 0.98 were
281 systematically excluded from the representation.

282 For each *in vitro* and *in vivo* experiment, the coil was held in position with adhesive tape and
283 not tilted during acquisitions. The EC was oriented in such a way to keep the B_1 of the EC
284 perpendicular to both static B_0 and transmit RF B_1 magnetic fields. Hence maximum
285 sensitivity and geometric decoupling are ensured respectively. As the colon natural behavior

286 is to fold, the EC is always encompassed by colon structures ensuring almost uniform radial
287 signal intensity.

288

289 **RESULTS:**

290 An endoluminal MR coil, fitting the constraints for *in vivo* experimentation on mice (colon
291 and rectum walls assessment) was designed and built. The prototypes are waterproof,
292 reusable, biocompatible (with the investigated environment) and can be tuned/matched to the
293 appropriate resonance frequency. The measured loaded Q-factor (Q_L) of the coil was 32 and
294 the coupling coefficient was found equal to 1.25. This leads to a value of 72 for the unloaded
295 Q-factor. The adaptation, at the 200.13 MHz working frequency in loading conditions was
296 50.03 Ohms. The decoupling efficiency of the EC was tested using a VNA. When the pin
297 diode is activated, the resonance frequency is shifted to 150 MHz and the isolation at the
298 resonance frequency reach -43 dB.

299 The EC provide a higher SNR in the close vicinity of the coil than the one obtained with
300 quadrature volume birdcage coil. The EC geometry and dimensions fit with the use of the
301 volume birdcage coil (72 mm inner diameter), without causing interferences and/or impacting
302 the image quality. The absence of signal highlights in the close vicinity of the EC was
303 confirmed when acquiring images with the body coil. Indeed, the continuously decoupled EC,
304 not impacting the image around loop coil, was attested the correct functioning and efficacy of
305 the decoupling circuit. The results of the SNR obtained with the EC compared with the
306 QVBC acquired on phantom solutions are shown in figure 2. In receive mode, the SNR profile
307 of the EC was much higher than the one achieved with the QVBC up to 3 mm apart from the
308 coil center. SNR profiles plotted in figure 2 were corrected regarding the voxel size,
309 bandwidth and number of excitations for a straightforward comparison. The EC SNR gain is
310 10 times greater at the close proximity and reaches the SNR of the QVBC at approximately
311 3 mm from the center.

312 A precise measurement of the structures observable in the loop-coil field of view was
313 achieved on the phantom constituted with calibrated optical fibers (figure 3). Optical

314 fibers diameters were measured with a standard deviation of $\pm 6.3 \mu\text{m}$ using the ImageJ
315 software and then compared with a digital caliper (nominal precision $\pm 10 \mu\text{m}$).
316 Experiments led on vegetables have shown the feasibility to obtain high spatial resolution
317 images and depict structural details. It is possible to distinguish the lamellar structures of the
318 onion to approximately 3 mm of the coil center (figure 4). White arrows on figure 4 localize the
319 same thin slice of the onion obtained with the VC (figure 4a) and with the EC (figure 4b and
320 4c) at two different spatial resolutions (different SNR).

321

322 ***In vivo* Experiments**

323 The EC geometry fits the mouse anatomy and is adapted to *in vivo* experiments. Once the
324 mouse is anesthetized, the insertion of the EC performed by an experimented
325 gastroenterologist is simple and harmless for the animal. The animal's recovery time is short
326 and no signs of prostration and/or pain were observed during the following few hours in
327 accordance with the French legislation. Images acquired *in vivo* show a very good quality
328 (figure 5), in terms of contrast and high spatial resolution. The use of the QVBC does not allow
329 a correct visualization of colon walls due to limited achievable spatial resolution. Whereas the
330 SNR gain provided by the EC is used to increase spatial resolution and to depict nicely the
331 mouse rectum wall layers and surrounding structures. On figure 5b, the map ratio of
332 $\text{SNR}_{\text{EC}}/\text{SNR}_{\text{QVBC}}$ is overlaid on MR images and undoubtedly illustrates the improved SNR
333 area given by the EC. The white arrow on figure 5a1 and 5c locates a blood vessel used for
334 co-localization. The examination with the EC gives a better visualization of colorectal wall
335 layers and surrounding structures (figure 5d and 5e). White arrows locate also the mucosa –
336 submucosa complex. Using such a coil allows to increase spatial resolution up to $39 \mu\text{m}$ in-
337 plane resolution (with $234 \mu\text{m}$ slice thickness, see figure 6a and 6b). It is then possible to well

338 distinguish the mucosa complex in details. ① is the mucosa, ② the submucosa and ③ the
339 muscularis externa. On figure 6b, ④ locates a thin muscle layer.

340 The T1- and T2-values of structures around the EC can be seen on figure 7. The maps have
341 been calculated and plotted with an estimation of the fit quality to ensure reliable values. It is
342 worth noting that this parametric procedure removes the strong signal intensity decay that
343 could lead to misinterpretation on the magnitude images. T1- and T2-maps plotted from two
344 different slices illustrate different structures; ① identifies a muscle structure and ② the colon
345 wall. The averaged T1 relaxation times were measured at $800 \text{ ms} \pm 100 \text{ ms}$ and
346 $1200 \text{ ms} \pm 200 \text{ ms}$ respectively. Then, looking at the T2 maps, mucosa layer and muscularis
347 externa are clearly differentiable (③ and ④ on figure 7). The T2 relaxation times are nearly
348 identical, $80 \text{ ms} \pm 10 \text{ ms}$ for both structures. Finally, * locates the submucosa which tends to
349 have lower T2 values ($50 \text{ ms} \pm 10 \text{ ms}$). The fit quality maps show a reproducible method for
350 T1- and T2-values with only a few points excluded in the field-of-view considered.

351

352 **DISCUSSION:**

353

354 EC have been used since the late eighties [41] but essentially for visualizing human prostate
355 and rectum regions [42–45]. Currently, the major problem lies in the heat induce by the RF
356 current into conductors. Several studies have shown the potential of using RF traps to reduce
357 this increase in temperature [24, 26, 46]. Optical transmission and optical decoupling system
358 have also been proposed in order to replace conventional coaxial cable [47, 48]. More
359 recently, the exploration of metamaterials have open new perspectives for alternative ways of
360 RF signal transmission [49]. These metamaterials could overcome several coaxial cable
361 disadvantages such as high propagation loss or heating along the conductor in the presence of
362 electrical fields. But also, reaching the Human colon is difficult due to the 90° angle and
363 assessing higher structures in the colon may require flexible endorectal MR probes. Other
364 studies have shown the high potential of using ECson preclinical models such as pigs [50],
365 rabbits [16, 19] and rats [15]. But, it is the first reported study assessing colon and rectum
366 walls using dedicated endorectal coils on a mouse model of colitis (inflammation evolving
367 into cancer).

368 In this study, the feasibility to design an EC for small animal colon wall imaging such as mice
369 was demonstrated. It has been shown that EC can provide typical 40 μm in-plane pixel images
370 with a slice thickness of 234 μm along digestive tract. External volume coils provide less
371 detailed images in similar conditions (same sequence parameters and position). It enables the
372 visualization of colon wall layers and deeper structures with a spatial resolution and SNR not
373 achievable with quadrature volume birdcage coil dedicated to mice gastrointestinal imaging.

374 For decoupling the EC during the emission of radiofrequencies RF pulses, a parallel
375 decoupling circuit was used. This choice was made to decrease the total resistance of the coil.

376 Indeed, regarding the coil's dimensions and components, one third to one half of the total

377 circuit resistance is due to the PIN diode characteristics alone.Placing the PIN diode in series
378 leads in higher decoupling efficiency but decreases the quality factor and the SNR as well.
379 When the PIN diode is placed in parallel of the tuning capacitor, the resistance is lowered.
380 The quality factor of the coil is improvedbut the decoupling efficiency is reduced. The PIN
381 diode is not entirely shutting down the loop coil and a weak fraction of the radiofrequency
382 signal can still go through into the loop.In principle a coil having one or two parallel PIN
383 diodes mounted in series with the loop would benefit from a better decoupling performance.
384 Even if this solution is feasible for *in vitro* experiments it is not compatible with *in vivo*
385 experiments.PIN diode used here are bigger components than case A ATC capacitors. Several
386 PIN diodes on the coil will result in blocking the access to trimmer capacitors.
387 Using those trimmer capacitors help for tuning/matching the coil at the desired frequency but
388 this kind of component has a poor life time, due to their mechanism working with a
389 screwdriver, and had to be changed regularly. Usually, trimmer capacitors are linked to
390 insulating sticks for tuning and matching. In the case of small coils it is difficult to have such
391 a configuration.

392 A heat shrink coating covers the EC during *in vivo* or *in vitro* experiments to prevent the
393 sensor from immediate short-circuit risk. Consequently,the copper tracks are isolated from the
394 surrounding mediumbut this protection layer weakens the maximum SNR achievable in the
395 close vicinity of the coil. Using a thinner protection could improve the SNR close to the
396 coil.Besides, the EC is wrapped with PTFE to protect the electronic circuit during *in vivo*
397 experiments:as the coil is used in wet environment, long-term oxidation of the copper tracks
398 can appear if the PTFE is not removed after each use and the EC not properly dried.
399 Oxidation could lead to short-circuits, deterioration of the copper tracks and/or components
400 and degradation of transmission line properties.A protective plastic cover will be designed
401 and printed to improve protection. SNR comparisons could not be achieved using the QVBC

402 at the exact same position due to the absence of decoupling circuit on this coil. The
403 comparison was then done sequentially slice by slice and correlated with images acquired
404 with the EC. Mouse's body examination would hardly be done with the available 70 mm inner
405 diameter birdcage coil. However, the use of a 40 mm inner diameter linear birdcage coil with
406 active decoupling system would easily allow switching between EC and volume coil. Beside
407 the easier and straightforward comparison in SNR, this setup would allow to acquire very
408 local images of the colon as well as more regional images of the mouse. This setup would be a
409 considerable way of improvement.

410 The phantom containing optical fibers was useful to assess the size of structures that could be
411 observed (from 150 μm to 1 mm) in the EC FOV. On the figure 3, optical fibers seem to be
412 equally distributed around the EC. As optical fibers fell down to the bottom of the container the
413 upper part of the phantom was not containing enough fibers. More of them will have to be
414 added to distribute correctly optical fibers around the sensor. Despite the fact that the
415 sequences chosen for imaging the phantom had a slice thickness of 234 μm , no partial volume
416 effect was observed when measuring outer diameter of the optical fibers.

417 For the experimentations done on vegetables, onions have been chosen for their structure.
418 Despite the fact that onions present very thin lamellar patterns, it can be assimilated to a semi-
419 rigid material. The molecules of water are constrained by their environment. So, when looking
420 closely to the lamellar structure of this vegetable, it appears that air gaps are located between
421 each slice. This causes some susceptibility artefacts. Moreover, the slice position chosen for
422 the comparison was not exactly the same than the one obtained with the VC. To be able to
423 localize the same structures between body coil images and EC images, the VC was used
424 instead of the QVBC. The SNR of the VC allows the overall visualization of several layers of
425 the vegetable. But to depict lamellar structure, the VC is inappropriate due to insufficient
426 SNR. The use of the EC increases drastically the local SNR and fine structures can be

427 visualized. But it also causes a highlight on the image, in the close vicinity of the coil. To
428 obtain the same details with the QVBC, the same sequence was done using six averages; the
429 acquisition time was increase to 1h15min.

430 *In vivo* acquisitions show a huge improvement in the differentiation of colon wall
431 layerscomparedto the QVBC. The designed EC fits with the straight configuration of the
432 mouse colon. Indeed, human colon presents curves which cannot be passed using such a rigid
433 coil. For one of the healthy mouse, the colon was sampled for further analyzes.During the
434 dissection, the length, average diameter and thickness of the colon were approximately
435 measured, using a digital caliper, to optimize the coil loop.

436 The protocol duration developed for the need of the study wasshort enough (~38 min) to
437 ensure the safe examination and recovery of the animal. It provides anatomical and parametric
438 images (T1 and T2 values). Three scout sequences with orthogonal plane orientationswere
439 first done with the VC in emission/reception mode. Acquisitions were compared between
440 images acquired with and without a trigger deviceusing a respiratory sensor place on the
441 lower part of the abdomen. Though respiratory movement is ample and cardiac beats are
442 rapid, those movements are far from the colon and no significant differences were observed.
443 So, no sequence triggering was performed in order to reduce the acquisition time.
444 Nevertheless, colon can be affected by peristaltic movements.These movements have been
445 evaluated using an optical system developed for this purpose. Movements of colon walls are
446 slow, not regular and limited in amplitude.The degradation induced by this motion on image
447 quality is thus difficult to evaluate.A further analysis will be done to quantify this movement
448 and see the influence on MR images.

449 The EC provides a high SNR in its close vicinity but the SNR drops down heavily. Up to
450 3 mmfrom the center, the SNR is higher than the one with the QVBC, further the sensitivity
451 of the EC begins very poor. The colon wall thickness was measuresin the range of

452 0.2to0.5 mm (0.3 – 1mm in the literature [28, 51]). Regions of interest, such as colon walls,
453 are closely located to the loop coil where the EC provides a very high SNR.Looking further
454 the two first millimeters is not required for the purpose of this study.On figure 6, the in-plane
455 pixel size was reduced (~39 μm pixel width with a slice thickness of 234 μm). As the SNR is
456 decreasing with the improvement of spatial resolution, the gain in SNR provided by EC is
457 used to define the best compromise between pixel size and signal intensity. As the QVBC
458 does not possess a decoupling circuit, the colocalization was done using anatomical markers.
459 Blood vessels are convenient to localize the slice position. The mouse bladder and vertebrae
460 can also be used as convenient landmarks.

461 Even if an optical endoscopic control exam is realized before inserting the coil into the mouse
462 rectum, sometimes the lumen is still filled with feces and other natural substances. Those
463 feces tend to drastically decrease the signal leading in an important loss of contrast around the
464 feces. The systematic endoscopic control combined with a medication controlling the
465 peristaltic movement (loperamide for example) could help to reduce the presence of feces in
466 the lumen.During the evolution of the pathology, bleeding can also appear. When the EC is
467 pulled out from the colon the presence of blood is sometimes noticed. This also induces
468 distortion into the image quality and has to be taken into account for image processing.

469 Computed parametric T1- and T2-maps remove the strong SNR decay associated with the use
470 of the EC. It is a fact that these strong intensity variations reduce the way the image is ridden
471 compare to uniform signal intensity (provided by a QVBC for example).The T1 and T2
472 relaxation times obtained on the colon walls present an important standard deviation from the
473 mean value. This is due to heterogeneity and size of the *in vivo* structures but also depends on
474 the fit quality. Theoretically, in each pixel it is possible to obtain a value of the T1 and T2.
475 Practically, some fits present a coefficient of determination too low to be taken into account. A
476 part of the problem is due to the high and rapid variation of structures observed *in vivo*.

477 Moreover, structures are very thin and can be essentially made of fat (for deeper structures for
478 example). The non-significant values are removed from the results and can cause holes in the
479 maps. A further study will be to evaluate the influence of the number and values of flip angles
480 on fit quality. The 0.98 threshold here is chosen following what anatomical structures need to
481 be seen in the EC FOV. It corresponds to a setting neither too general nor drastic. Information
482 furnished by a fit quality of 0.98 are corresponding to the colon wall and surrounding structures.
483 When designing the coil, there were no considerations of heating and/or specific absorption
484 rate (SAR) taken into account. Indeed, during MR procedures, the radiofrequency power
485 transmitted (from the emission coil) for imaging is turned into heat through resistive losses.
486 Furthermore, when a conductor is placed within the imaging volume (as with the use of ECs)
487 the RF electrical field accompanying the RF magnetic field pulses induces currents that can
488 cause local concentration of the SAR [25, 26, 52, 53]. In our case, the loop can be considered
489 as a wire but the quarter wavelength (at 200 MHz) is much higher than the length of the loop.
490 It has been assumed that wire lengths less than a quarter wavelength are generally safe.
491 The presence of an active decoupling circuit is also mandatory to reduce SAR
492 concentration [24]. Further work will be to combine the EC with magnetic resonance
493 spectroscopy (MRS) in the colon wall. MRS could provide information on the biochemical
494 composition of deep tissue layers. Quantitative analysis of the biochemical contents could
495 also bring new markers to improve the measurements. But several challenges still lie ahead,
496 such as strong B_0 inhomogeneities and phase shift due to the difference of magnetic
497 susceptibility between air in the lumen and wall tissues.

498 In order to exploit the described work, a longitudinal follow up over six months involving
499 24 mice will be performed to explore *in vivo* the gastrointestinal wall in its entire depth. MR
500 ECs open new perspectives as a minimally invasive technique to characterize colorectal

501 cancer lesions and inflammatory bowel disease and then, offer a new technique to better
502 understand the development of the colon wall pathologies.

503

504 **CONCLUSION:**

505 In conclusion, an endoluminal coil was developed for imaging the colon and rectum walls on
506 a mouse model of colitis. The strong local SNR increase provided by the use of such coils
507 allows imaging the gastrointestinal tract at very high spatial resolution (up to approximately
508 40 μm in plane resolution with a slice thickness of 234 μm). Associated to a dedicated
509 protocol, it provides details in deep still thin structures of colon wall.

510

511 **Author's Contribution:**

512

513 DOREZ: Protocol/project development, data collection or management and data analysis

514 SABLONG: Protocol/Project development, data collection

515 CANAPLE: Protocol/project development

516 SAINT-JALMES: Protocol/project development

517 GAILLARD: Data collection

518 MOUSSATA: Protocol/project development, data collection or management

519 BEUF: Protocol/project development, data collection or management

520

521 **COMPLIANCE WITH ETHICAL STANDARDS:**

522 **Disclosure of potential conflicts of interest:** the authors declare that they have no conflict of
523 interest.

524

525 **Research involving animals:** all applicable international, national, and/or institutional
526 guidelines for the care and use of animals were followed.

527 All procedures performed in studies involving animals were in accordance with the ethical
528 standards of the institution or practice at which the studies were conducted.

529

530 **REFERENCES**

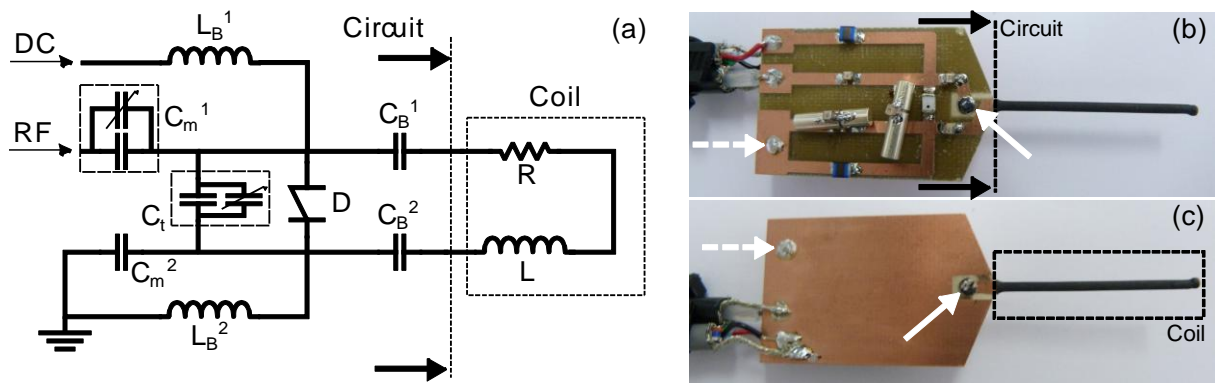
- 531 1. Bray F, Jemal A, Grey N, Ferlay J, Forman D (2012) Global cancer transitions according to the
532 Human Development Index (2008–2030): a population-based study. *Lancet Oncol* 13:790–
533 801.
- 534 2. Jemal A, Bray F, Center MM, Ferlay J, Ward E, Forman D (2011) Global cancer statistics. *CA Cancer J*
535 *Clin* 61:69–90.
- 536 3. Siegel R, DeSantis C, Jemal A (2014) Colorectal cancer statistics, 2014. *CA Cancer J Clin* 64:104–117.
- 537 4. O’Connell JB, Maggard MA, Ko CY (2004) Colon Cancer Survival Rates With the New American Joint
538 Committee on Cancer Sixth Edition Staging. *J Natl Cancer Inst* 96:1420–1425.
- 539 5. Takayama T, Miyanishi K, Hayashi T, Sato Y, Niitsu Y (2006) Colorectal cancer: genetics of
540 development and metastasis. *J Gastroenterol* 41:185–192.
- 541 6. Bisognin A, Pizzini S, Perilli L, Esposito G, Mocellin S, Nitti D, Zanovello P, Bortoluzzi S, Mandruzzato
542 S (2014) An integrative framework identifies alternative splicing events in colorectal cancer
543 development. *Mol Oncol* 8:129–141.
- 544 7. Fearon ER (2011) Molecular Genetics of Colorectal Cancer. *Annu Rev Pathol Mech Dis* 6:479–507.
- 545 8. Vanagunas A, Lin DE, Stryker SJ (2004) Accuracy of Endoscopic Ultrasound for Restaging Rectal
546 Cancer Following Neoadjuvant Chemoradiation Therapy. *Am J Gastroenterol* 99:109–112.
- 547 9. Puli SR, Reddy JBK, Bechtold ML, Choudhary A, Antillon MR, Brugge WR (2009) Accuracy of
548 Endoscopic Ultrasound to Diagnose Nodal Invasion by Rectal Cancers: A Meta-Analysis and
549 Systematic Review. *Ann Surg Oncol* 16:1255–1265.
- 550 10. Puli SR, Bechtold ML, Reddy JBK, Choudhary A, Antillon MR (2010) Can Endoscopic Ultrasound
551 Predict Early Rectal Cancers That Can Be Resected Endoscopically? A Meta-Analysis and
552 Systematic Review. *Dig Dis Sci* 55:1221–1229.
- 553 11. Puli SR, Bechtold ML, Reddy JBK, Choudhary A, Antillon MR, Brugge WR (2009) How Good is
554 Endoscopic Ultrasound in Differentiating Various T Stages of Rectal Cancer? Meta-Analysis
555 and Systematic Review. *Ann Surg Oncol* 16:254–265.
- 556 12. Vander Noot MR, Eloubeidi MA, Chen VK, Eltoum I, Jhala D, Jhala N, Syed S, Chhieng DC (2004)
557 Diagnosis of gastrointestinal tract lesions by endoscopic ultrasound-guided fine-needle
558 aspiration biopsy. *Cancer* 102:157–163.
- 559 13. Hurlstone DP, Brown S, Cross SS, Shorthouse AJ, Sanders DS (2005) Endoscopic Ultrasound
560 Miniprobe Staging of Colorectal Cancer: Can Management Be Modified? *Endoscopy* 37:710–
561 714.
- 562 14. Hurlstone DP, Brown S, Cross SS, Shorthouse AJ, Sanders DS (2005) High magnification
563 chromoscopic colonoscopy or high frequency 20 MHz mini probe endoscopic ultrasound
564 staging for early colorectal neoplasia: a comparative prospective analysis. *Gut* 54:1585–1589.
- 565 15. Pilleul F, Beuf O, Armenean M, Scoazec JY, Valette PJ, Saint-Jalmes H (2004) In vitro rat colonic
566 wall imaging with MR endoluminal coil: Feasibility study and histologic correlations1. *Acad*
567 *Radiol* 11:795–801.

- 568 16. Beuf O, Pilleul F, Armenean M, Hadour G, Saint-Jalmes H (2004) In vivo colon wall imaging using
569 endoluminal coils: Feasibility study on rabbits. *J Magn Reson Imaging* 20:90–96.
- 570 17. Maldjian C, Smith R, Kilger A, Schnall M, Ginsberg G, Kochman M (2000) Endorectal surface coil
571 MR imaging as a staging technique for rectal carcinoma: a comparison study to rectal
572 endosonography. *Abdom Imaging* 25:75–80.
- 573 18. Syms R, Young I, Wadsworth C, Taylor-Robinson S, Rea M (2013) Magnetic Resonance Imaging
574 Duodenoscopy. *IEEE Trans Biomed Eng* 60:3458–3467.
- 575 19. Pilleul F, Beuf O, Godefroy C, Scoazec J-Y, Armenean M, Armenean C, Perrin E, Valette P-J, Jalmes
576 HS (2005) High-resolution MR imaging appearance of colonic tissue in rabbits using an
577 endoluminal coil. *Magn Reson Mater Phy* 18:238–244.
- 578 20. Klessen C, Rogalla P, Taupitz M (2007) Local staging of rectal cancer: the current role of MRI. *Eur*
579 *Radiol* 17:379–389.
- 580 21. Beaumont C, Pandey T, Gaines Fricke R, Laryea J, Jambhekar K (2013) MR Evaluation of Rectal
581 Cancer: Current Concepts. *Curr Probl Diagn Radiol* 42:99–112.
- 582 22. Armenean M, Beuf O, Pilleul F, Saint-Jalmes H (2001) Endoluminal loop radiofrequency coils for
583 gastrointestinal wall imaging. *Proc. 23rd Annu. Int. Conf. IEEE Eng. Med. Biol. Soc.* pp 3052–
584 3055
- 585 23. Armenean M, Beuf O, Pilleul F, Saint-Jalmes H (2004) Optimization of endoluminal loop
586 radiofrequency coils for gastrointestinal wall MR imaging. *IEEE Sens J* 4:57–64.
- 587 24. Ladd ME, Quick HH (2000) Reduction of resonant RF heating in intravascular catheters using
588 coaxial chokes. *Magn Reson Med* 43:615–619.
- 589 25. Nitz WR, Oppelt A, Renz W, Manke C, Lenhart M, Link J (2001) On the heating of linear conductive
590 structures as guide wires and catheters in interventional MRI. *J Magn Reson Imaging* 13:105–
591 114.
- 592 26. Shellock FG (2000) Radiofrequency Energy-Induced Heating During MR Procedures: A Review. *J*
593 *Magn Reson Imaging* 12:30–36.
- 594 27. Gauss R, Wong E (2009) RF traps for radio frequency coils used in MRI. U.S. Patent No. 7,622,928.
- 595 28. Tanaka T, Kohno H, Suzuki R, Yamada Y, Sugie S, Mori H (2003) A novel inflammation-related
596 mouse colon carcinogenesis model induced by azoxymethane and dextran sodium sulfate.
597 *Cancer Sci* 94:965–973.
- 598 29. Aychek T, Vandoorne K, Brenner O, Jung S, Neeman M (2011) Quantitative analysis of
599 intravenously administered contrast media reveals changes in vascular barrier functions in a
600 murine colitis model. *Magn Reson Med* 66:235–243.
- 601 30. Atalar E, Bottomley PA, Ocali O, Correia LC, Kelemen MD, Lima JA, Zerhouni EA (1996) High
602 resolution intravascular MRI and MRS by using a catheter receiver coil. *Magn Reson Med*
603 36:596–605.
- 604 31. Verret JM, Pilleul F, Rabrait C, Beuf O (2012) RF heating reduction associated to an MR
605 endoluminal coil at 3T. *ESMRMB 2012 29th Annu. Sci. Meet. Toulouse*, p 143

- 606 32. Komárek V (2012) Chapter 2.2 - Gross Anatomy. In: Hedrich HJ (ed) Lab. Mouse Second Ed.
607 Academic Press, Boston, pp 145–159
- 608 33. Doty FD, Entzminger G, Kulkarni J, Pamarthy K, Staab JP (2007) Radio frequency coil technology
609 for small-animal MRI. *NMR Biomed* 20:304–325.
- 610 34. Hoult DI, Richards RE (1976) The signal-to-noise ratio of the nuclear magnetic resonance
611 experiment. *J Magn Reson* 24:71–85.
- 612 35. Kajfez D, Hwan EJ (1984) Q-Factor Measurement with Network Analyzer. *IEEE Trans Microw*
613 *Theory Tech* 32:666–670.
- 614 36. Ginzton EL (1958) Microwave Q Measurements in the Presence of Coupling Losses. *IRE Trans*
615 *Microw Theory Tech* 6:383–389.
- 616 37. Cheng H-LM, Wright GA (2006) Rapid high-resolution T1 mapping by variable flip angles: Accurate
617 and precise measurements in the presence of radiofrequency field inhomogeneity. *Magn*
618 *Reson Med* 55:566–574.
- 619 38. Hashemi RH, Bradley WG, Lisanti CJ (2012) MRI: The Basics. Lippincott Williams & Wilkins
- 620 39. Rasband WS, et al. (1997) & ImageJ. Bethesda, Md, USA
- 621 40. Gibbs P, Tozer DJ, Liney GP, Turnbull LW (2001) Comparison of quantitative T2 mapping and
622 diffusion-weighted imaging in the normal and pathologic prostate. *Magn Reson Med*
623 46:1054–1058.
- 624 41. Schnall MD, Lenkinski RE, Pollack HM, Imai Y, Kressel HY (1989) Prostate: MR imaging with an
625 endorectal surface coil. *Radiology* 172:570–574.
- 626 42. Stoker J, Rociu E (1999) Endoluminal MR imaging of diseases of the anus and rectum. *Semin*
627 *Ultrasound CT MRI* 20:47–55.
- 628 43. Sathyanarayana S, Bottomley PA (2009) MRI endoscopy using intrinsically localized probes. *Med*
629 *Phys* 36:908–919.
- 630 44. Zagoria RJ, Schlarb CA, Ott DJ, Bechtold RE, Wolfman NT, Scharling ES, Chen MYM, Loggie BW
631 (1997) Assessment of rectal tumor infiltration utilizing endorectal MR imaging and
632 comparison with endoscopic rectal sonography. *J Surg Oncol* 64:312–317.
- 633 45. D'Amico AV, Schnall M, Whittington R, Malkowicz SB, Schultz D, Tomaszewski JE, Wein A (1998)
634 Endorectal coil magnetic resonance imaging identifies locally advanced prostate cancer in
635 select patients with clinically localized disease. *Urology* 51:449–454.
- 636 46. Verret JM, Rabrait C, Pilleul F, Beuf O (2012) Réalisation de capteurs endoluminaux en Imagerie
637 de Résonance Magnétique à 3T: performances et sécurité. Proc. 1st Meet. Société Fr.
638 Résonance Magnétique En Biol. Médecine. Marseille, p 1
- 639 47. Ayde R, Gaborit G, Jarrige P, Duvillaret L, Sablong R, Perrier A, Beuf O (2013) Potentialities of an
640 Electro-Optic Crystal Fed by Nuclear Magnetic Resonant Coil for Remote and Low-Invasive
641 Magnetic Field Characterization. *IEEE Sens J* 13:1274–1280.

- 642 48. Fandrey S, Weiss S, Muller J (2008) Development of an Active Intravascular MR Device With an
643 Optical Transmission System. *IEEE Trans Med Imaging* 27:1723–1727.
- 644 49. Syms R, Solymar L, Young IR (2010) Periodic Analysis of MR-Safe Transmission Lines. *IEEE J Sel Top*
645 *Quantum Electron* 16:433–440.
- 646 50. Thörmer G, Reiss-Zimmermann M, Otto J, Hoffmann K-T, Moche M, Garnov N, Kahn T, Busse H
647 (2013) Novel technique for MR elastography of the prostate using a modified standard
648 endorectal coil as actuator. *J Magn Reson Imaging* 37:1480–1485.
- 649 51. Larsson AE, Melgar S, Rehnström E, Michaëlsson E, Svensson L, Hockings P, Olsson LE (2006)
650 Magnetic resonance imaging of experimental mouse colitis and association with
651 inflammatory activity. *Inflamm Bowel Dis* 12:478–485.
- 652 52. Yeung CJ, Susil RC, Atalar E (2002) RF safety of wires in interventional MRI: using a safety index.
653 *Magn Reson Med* 47:187–193.
- 654 53. Konings MK, Bartels LW, Smits HFM, Bakker CJG (2000) Heating Around Intravascular Guidewires
655 by Resonating RF Waves. *J Magn Reson Imaging* 12:79–85.
- 656
- 657

658 LIST OF FIGURES

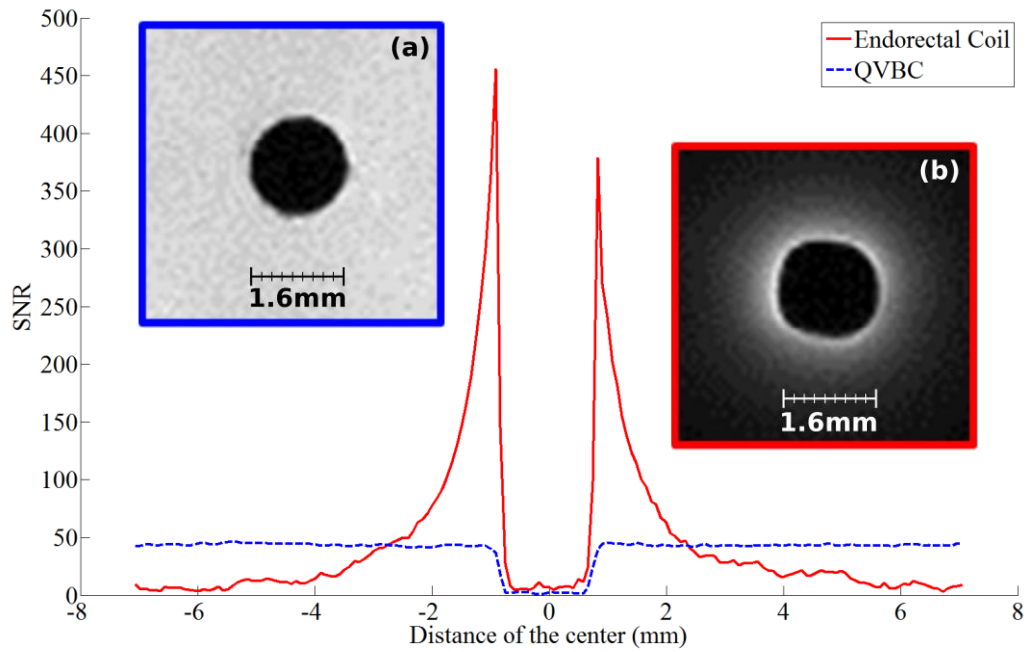


659

660 Legend of Fig1:

661 **Fig 1** (a) Electric scheme of the coil. The corresponding part between the scheme and the pictures are
 662 illustrated. (b) The upper face of the coil with the soldered components constitutes the RLC resonator.
 663 On (c) is represented the lower face of the prototype. Straight white arrow is the location of the plated
 664 drill between the two faces for connecting the electrical circuit to the coil. White dashed arrow is the
 665 location of the connection between the grounds (DC and RF) to the ground plane. Values of
 666 components are mentioned in Table 1

667

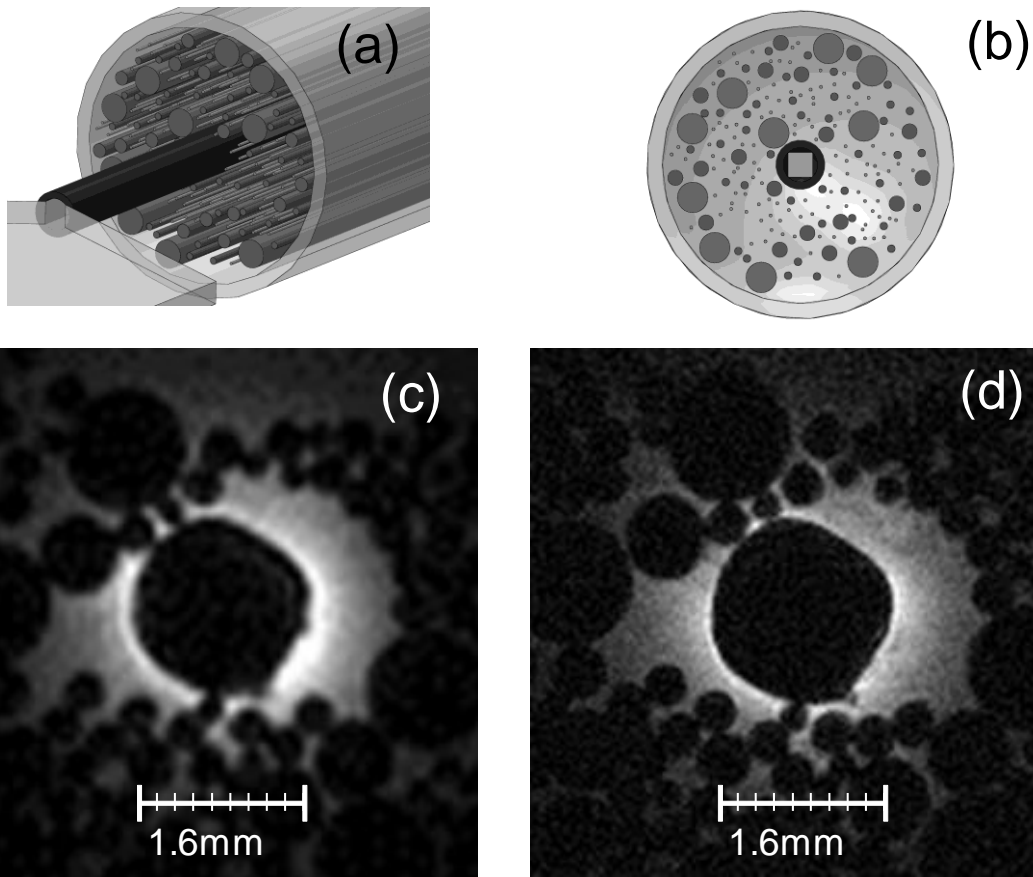


668

669 Legend of Fig 2:

670 **Fig 2** Comparison of the EC SNR profile (straight profile) and the QVBC SNR profile (dashed profile)
 671 obtained on a phantom containing 1.25 g/L NiSO₄ and 5 g/L NaCl. (a) is the image used for plotting
 672 the QVBC profile and (b) the image used for the EC profile. Close to the coil the SNR is drastically
 673 better than the one obtained with a dedicated quadrature birdcage coil

674

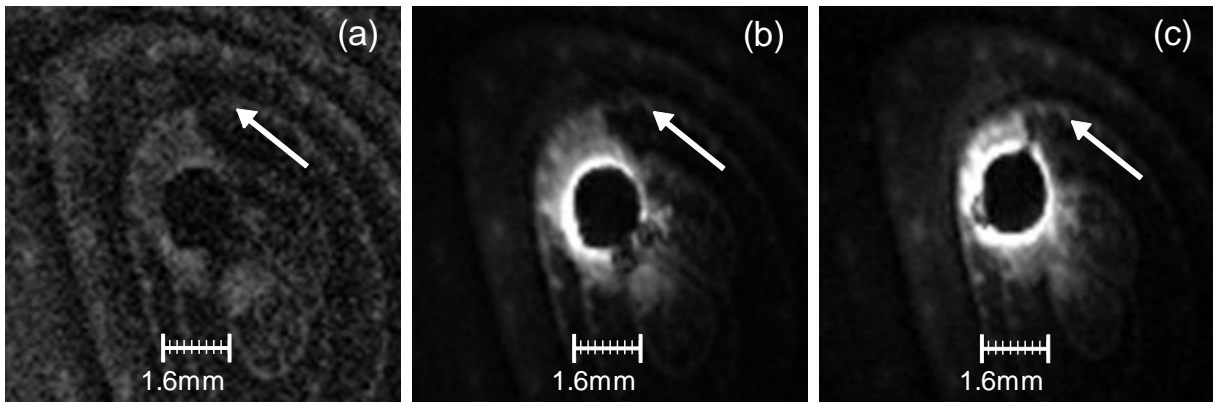


675

676 Legend of Fig 3:

677 **Fig 3** Images of the phantom created for the purpose of the experiments. (a) and (b) represent a
 678 reconstruction of the phantom containing optical fibers of different diameters. (c) and (d) are the
 679 corresponding MR images obtain with FLASH sequences at different voxel size ($50 \times 50 \mu\text{m}^2$ for (c) and
 680 $39 \times 39 \mu\text{m}^2$ (d)). The slice thickness was kept constant and equals to $234 \mu\text{m}$

681



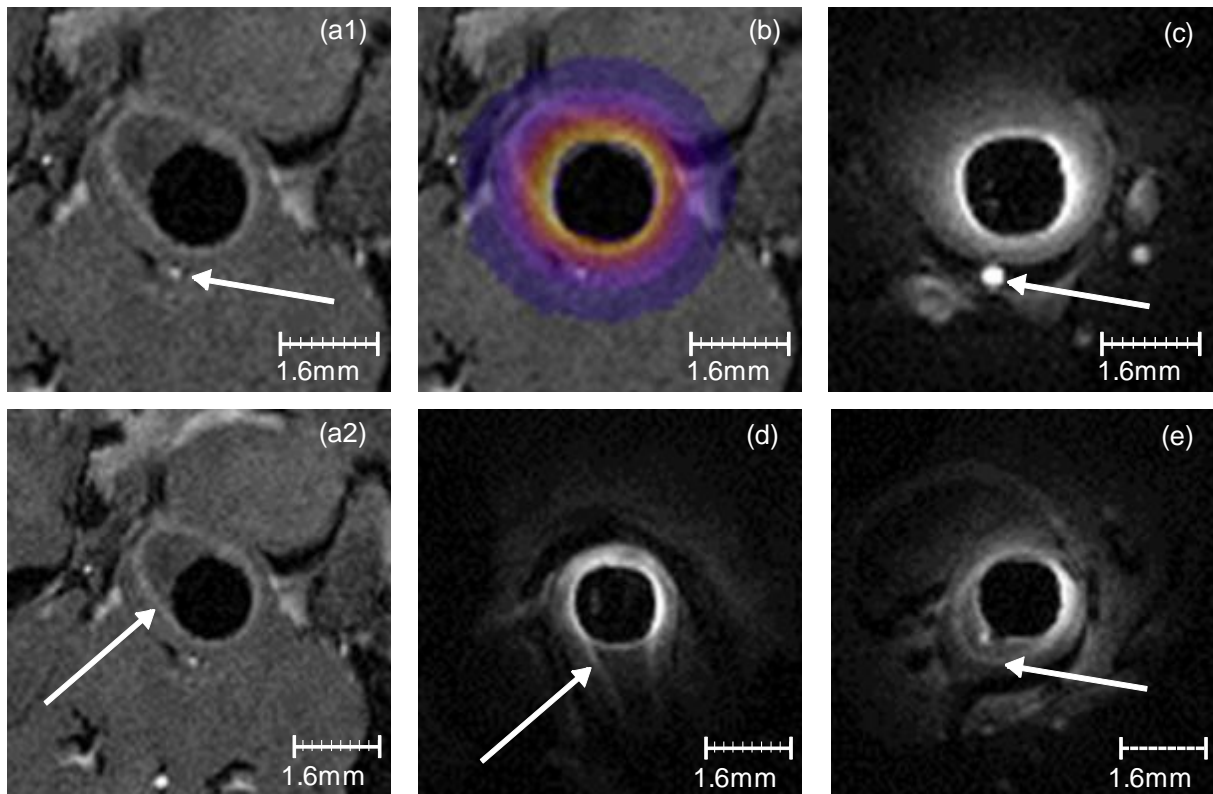
682

683 Legend of Fig 4:

684 **Fig 4** MR images of onion. (a) the volume coil was set in E/R mode, the lamellar structure represented
685 by the white arrow are not correctly distinguishable. Switching the configuration by setting the VC in
686 emission mode and the EC in reception mode the SNR and image quality are improved. On (b) the
687 voxel size was decrease up to $78 \times 104 \mu\text{m}^2$ lamellar surface can be depicted more easily. Finally, the
688 voxel size was reduced to $39 \times 39 \mu\text{m}^2$ on (c). Along the three MR images the slice thickness was set to
689 $234 \mu\text{m}$

690

691



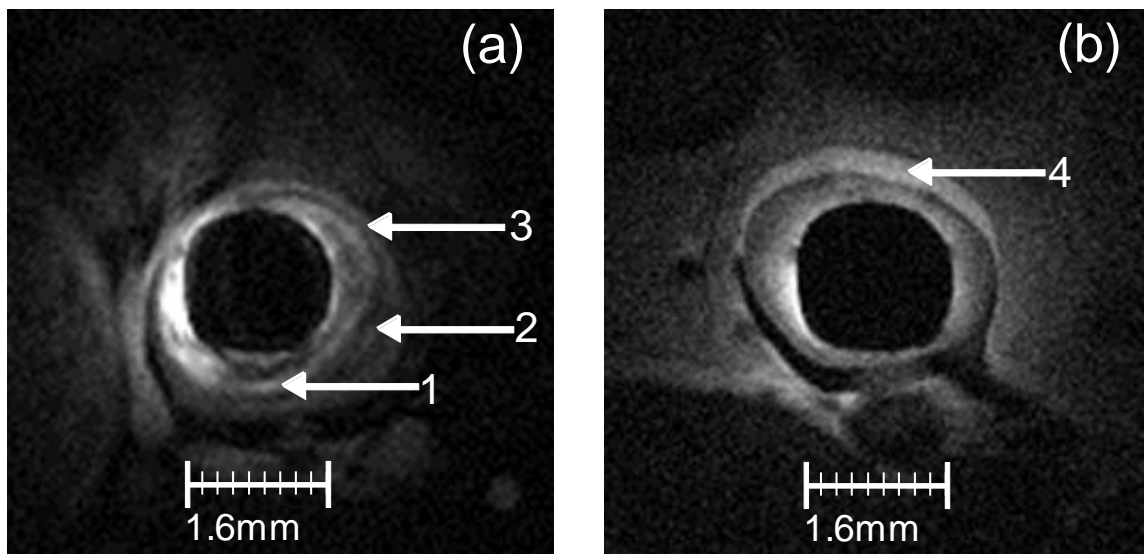
692

693 Legend of Fig 5:

694 **Fig 5** *in vivo* experiments were performed on a mouse model of colitis. MR images acquired with the
695 QVBC show blood vessels on (a1) and the colon wall on (a2) – white arrows. The SNR is too low to
696 correctly distinguish the colon wall layers in details. The use of the EC allows to increase the local
697 SNR. On (b) is represented the ratio between the SNR ratio of the QVBC and the EC. The EC FOV is
698 sufficient for the region of interest. On (c), white arrow locates the same blood vessel than on (a1) and
699 it is used for colocalization. (d) and (e) are showing the colon wall layer on different slices

700

701



702
703

Legend of Fig 6:

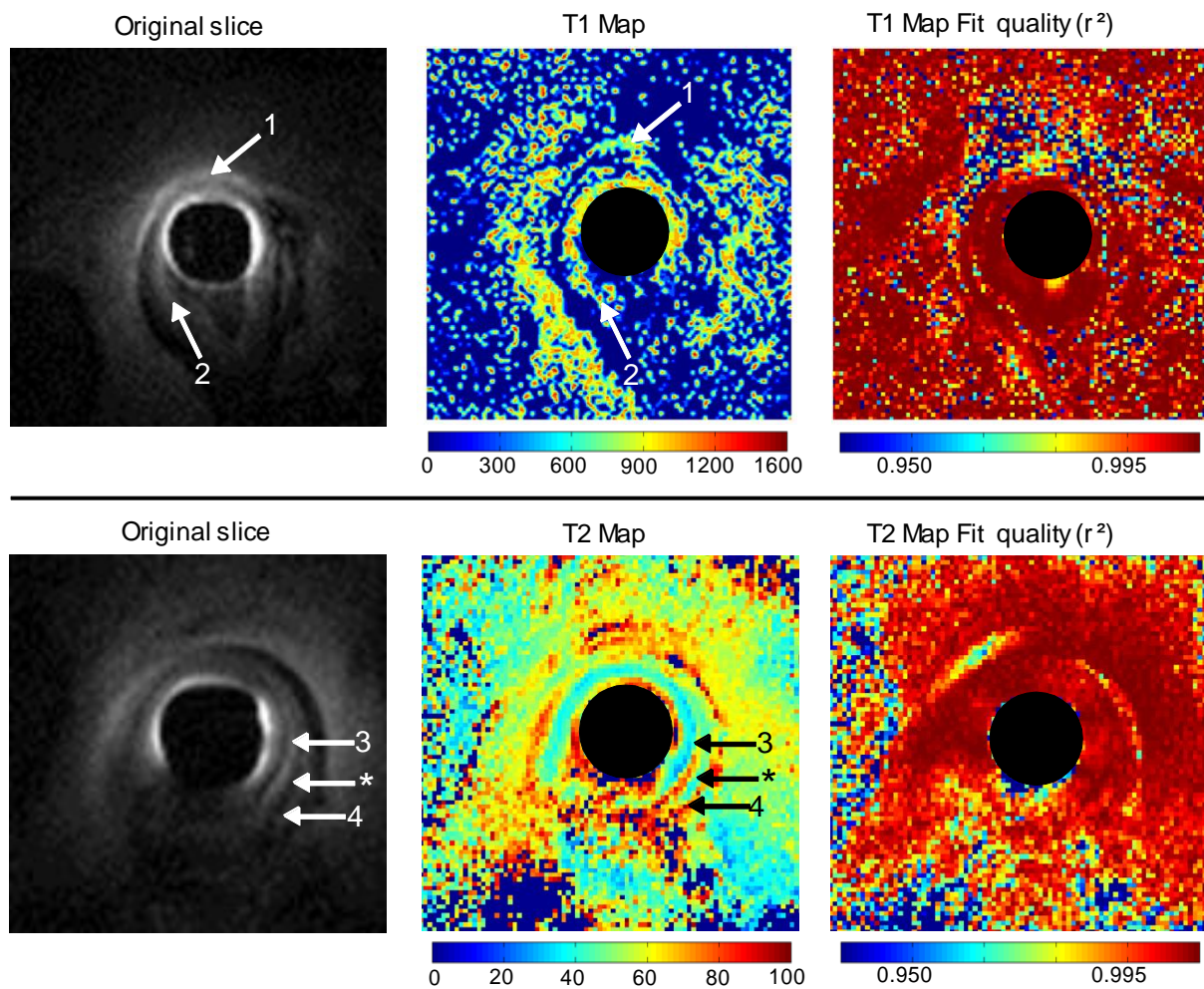
704 **Fig 6** From (a) to (b) the spatial resolution was increased up to $39 \times 39 \mu\text{m}^2$ (slice thickness of $234 \mu\text{m}$).

705 It is then possible to depict the colon wall complex in details. (1) refers to the mucosa, (2) to the

706 submucosa and (3) to the muscularis propria. (4) Represents a thin muscle layer closed to the coil. On

707 (b) the colon wall seems to have disappeared

708



710
 711 Legend of Fig 7:

712 **Fig 7** T1- and T2-maps obtained on different slices. (1) indicates the location of a thin muscle
 713 structure having T1 relaxation times lower than the ones observed on the colon wall (2). (3) and (4)
 714 represents two different layers (mucosa and muscularis propria) which nearly identical physiological
 715 constitutions so on with their respective T2 relaxation times. (*) locates the layer between the two
 716 previous one and show a very different T2 time

717

Table 1 Components used to build the endoluminal coil with values, manufacturers and references.

Function	Name	Value	Components
Tuning	Ct	22pF + 1pF	Non-variable non-magnetic capacitor
		from 0.8pF to 8pF	Non-magnetic trimmer capacitor
Matching	Cm1	5.6pF	Non-variable non-magnetic case A capacitor
		from 0.8pF to 8pF	Non-magnetic trimmer capacitor
	Cm2	5.6pF + 2.2pF + 1pF	Non-variable non-magnetic case A capacitor
Blocking	Cb1	100pF + 82pF	Non-variable non-magnetic case A capacitor
	Cb2	100pF + 82pF	Non-variable non-magnetic case A capacitor
Active decoupling	D	X	PIN diode
	LB1	1.2μH	Choke inductors
	LB2	1.2μH	Choke inductors

Table 2 Sequence and parameters used for the *in vivo* protocol. The scout sequences are not mentioned.

Sequence	Orientation	FOV (mm ²)	Slab/Slice Thickness (mm)	TR/TE (ms/ms)	Flip Angle (°)	Matrix	Voxel Size (μm ³)	Receive BW (kHz)	Acquisition Time
Flash 3D	Axial	16x16	1x15	20/6.653	15/20/25	192x192x64	83x83x234	25	8: 11'
FLASH 3D	Coronal	32x32	1x5	23.87/8.19	20	384x384x16	83x83x312	25	2: 26'
Multi TE	axial	10x10	6x1.5	2000/12,8+6x12,6	/	128x128x66	78x78x308	25	6: 24'

722

723

Table 3 Sequences used for the characterization of the EC and the assessment of the EC during *in vitro* experiments.

Sequence	Orientation	FOV (mm ²)	Slab Thickness (mm)	TR/TE (ms/ms)	Flip Angle (°)	Matrix	Voxel Size (μm ³)	Receive BW (kHz)	Acquisition Time
Flash 3D	Axial	16x16	1x15	20/6.653	20	192x192x64	83x83x234	25	8: 11'
FLASH 3D	axial	10x10	1x15	20/6.1	20	256x256x64	39x39x234	25	10: 55'

724